Measurement of Lorentzian linewidths by pulse propagation delay

A. Kasapi,* G. Y. Yin, Maneesh Jain, and S. E. Harris
Edward L. Ginzton Laboratory, Stanford University, Stanford, California 94305
(Received 22 December 1995)

Two related methods for determining the Lorentzian linewidth of one- and two-photon transitions in an atomic medium are presented. In each method, the linewidth is determined by the relationship between the energy transmission and propagation delay of a series of laser pulses sent through the medium; precise knowledge of the laser frequency, atom density, or matrix elements is not required. [S1050-2947(96)09106-8]

PACS number(s): 42.50.Gy, 32.70.Jz, 39.30.+w

INTRODUCTION

This paper presents two related methods for determining the Lorentzian linewidths of one- and two-photon transitions in atomic or molecular media. These methods were developed as diagnostic tools for electromagnetically induced transparency experiments in atomic lead [1], but are widely applicable to other media. In each method, the linewidth is determined by the relationship between the transmission and propagation delay of a series of laser pulses sent through the medium; neither method requires precisely known laser frequencies or a known atom density. These methods are particularly well suited to small volumes of atomic media (i.e., sidearm cells and heat pipes), where the one-photon transition of interest (or the one-photon component of the two-photon transition) is optically thick and the transitions are collisionally broadened. With an independent means to determine the linewidth of an optically thick one-photon transition, it becomes possible to make a robust spectroscopic determination of the atom density by measuring the optical absorption near the transition.

We begin by describing the procedure for determining the linewidth of a single-photon transition and experimentally illustrate the procedure using an atomic lead medium. We then present in Sec. II the procedure for determining the linewidth of a two-photon transition and illustrate the procedure using the same lead medium. Section III discusses general guidelines and limitations for using these two methods.

I. DETERMINATION OF THE LINEWIDTH OF A ONE-PHOTON TRANSITION

A schematic of the atomic transition is shown in Fig. 1(a). A weak monochromatic laser field $\mathcal{E}_p \exp(i\omega_p t)$ is tuned near the center frequency ω_{31} of the transition; we denote its detuning by $\Delta\omega_p \equiv \omega_{31} - \omega_p$. The transition is homogeneously broadened and has the Lorentzian linewidth [full width at half maximum (FWHM)] $2\gamma_3$; the susceptibility of the medium is then given by [2–4]

$$\chi = \frac{|\mu_{13}|^2 N}{\epsilon_0 \hbar}\left[\frac{\Delta\omega_p - j\gamma_3}{\gamma_3^3 + \Delta\omega_p^2}\right], \tag{1}$$

where μ_{13} is the matrix element of the transition for the particular field polarization used and N is the population of the ground state.

The energy transmission of the laser through the medium is given by

$$\frac{\mathcal{E}_{\text{out}}}{\mathcal{E}_{\text{in}}} = e^{-2\alpha(\omega_p)L}, \tag{2}$$

where L is the physical length of the medium through which the pulse is propagated and $\alpha(\omega_p)$ is the absorption coefficient of the electric field at its center frequency ω_p. The attenuation coefficient is determined from the susceptibility

$$\alpha(\omega_p) = -\frac{\omega_{31}}{2c}\text{Im}\chi(\omega_p). \tag{3}$$

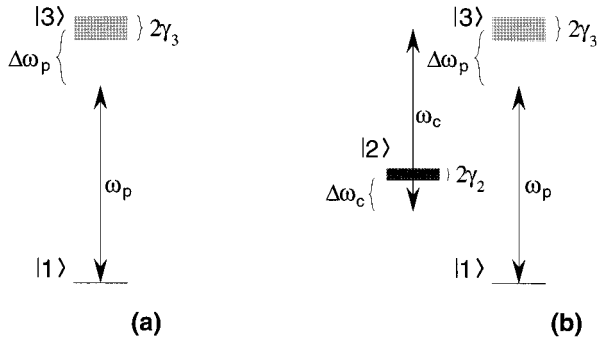

FIG. 1. (a) One-photon transition with ground state $|1\rangle$, upper state $|3\rangle$, and a Lorentzian FWHM linewidth $2\gamma_3$. Weak ''probe'' radiation of radian frequency ω_p is tuned near the transition with detuning $\Delta\omega_p$. (b) Two-photon transition consisting of the one-photon transition from (a) augmented by state $|2\rangle$. The (non-allowed) $|1\rangle \rightarrow |2\rangle$ transition has a linewidth of $2\gamma_2$. Strong ''coupling'' radiation with radian frequency ω_2 is tuned near the $|2\rangle \rightarrow |3\rangle$ transition; its detuning from the $|2\rangle \rightarrow |3\rangle$ transition is given by $\Delta\omega_c$. The two-photon detuning is thus given by $\Delta\omega_p - \Delta\omega_c$.

*Present address: Stanford Research Systems, Sunnyvale, CA 94089.

We henceforth confine our attention to the case where $\Delta\omega_p$ is sufficiently large that Eq. (3) can be accurately written as

$$\alpha(\omega_p)=\frac{|\mu_{13}|^2N}{\epsilon_0\hbar}\frac{\omega_{31}}{2c}\frac{\gamma_3}{\Delta\omega_p^2}. \tag{4}$$

The conditions under which this approximation gives accurate results are discussed in Sec. III.

The propagation delay $\tau_d=L/v_g$ of the pulse through the medium can be calculated from the group velocity v_g, which, in turn, is calculated from the susceptibility [5]

$$\frac{1}{v_g}=\frac{1}{c}+\frac{\omega_{31}}{2c}\left[\frac{\partial\ \mathrm{Re}(\chi)}{\partial\omega}\right]_{\omega_p}\cong\frac{1}{c}+\frac{|\mu_{13}|^2N}{\epsilon_0\hbar}\frac{\omega_{31}}{2}\frac{1}{\Delta\omega_p^2}. \tag{5}$$

We define the *excess delay* $\tau_e\equiv\tau_d-L/c$, which corresponds to the additional delay of a laser pulse propagating through a distance L in the medium compared to its delay propagating through the same distance in vacuum. It immediately follows that

$$\ln(\mathcal{E}_{\mathrm{out}}/\mathcal{E}_{\mathrm{in}})=-2\gamma_3\tau_e. \tag{6}$$

This equation has a simple physical interpretation: the energy of a pulse traveling much slower than the speed of light decays exponentially at twice the coherence decay rate of the $|1\rangle\rightarrow|3\rangle$ transition. This interpretation is consistent with the fact that, when a laser pulse travels through a medium with a slow group velocity, most of its energy is (reversibly) contained in the medium as coherent atomic excitation [6].

In principle, measuring $\mathcal{E}_{\mathrm{out}}/\mathcal{E}_{\mathrm{in}}$ and τ_e for a single laser pulse is sufficient to uniquely determine $2\gamma_3$. In practice, however, it is difficult to measure these quantities. It is more reasonable to measure $\mathcal{E}_{\mathrm{out}}$ and $\mathcal{E}_{\mathrm{in}}$ up to constant scale factors and to determine τ_e up to some fixed offset, so that Eq. (6) becomes

$$\ln(\mathcal{E}'_{\mathrm{out}}/\mathcal{E}'_{\mathrm{in}})=2\gamma_3\tau'_e+K, \tag{7}$$

where $\mathcal{E}'_{\mathrm{out}}=c_1\mathcal{E}_{\mathrm{out}}$ and $\mathcal{E}'_{\mathrm{in}}=c_2\mathcal{E}_{\mathrm{in}}$ indicate $\mathcal{E}_{\mathrm{out}}$ and $\mathcal{E}_{\mathrm{in}}$ measured up to fixed scale factors, $\tau'_e=\tau_e+\tau_0$ indicates τ_e measured up to a fixed time offset, and K is a constant offset.

To determine $2\gamma_3$, one need only cause $\mathcal{E}'_{\mathrm{out}}/\mathcal{E}'_{\mathrm{in}}$ and τ'_e to differ for two distinct pulses, yielding two equations from which the unknown constants $2\gamma_3$ and K can be determined. From Eqs. (4) and (5), this can be accomplished by varying either N, $\Delta\omega_p$, or both. Note that the actual detuning or variation in N need not be known; all that is required is to cause the pulse attenuation and delay to differ between two pulses.

The determination of $2\gamma_3$ can be made less susceptible to statistical fluctuations by measuring τ'_e and $\mathcal{E}'_{\mathrm{out}}/\mathcal{E}'_{\mathrm{in}}$ for many pulses of assorted detunings from the line center or at different atom densities N and plotting this pair of measurements for each pulse as a point on a graph where the y axis is $\ln(\mathcal{E}'_{\mathrm{out}}/\mathcal{E}'_{\mathrm{in}})$ and the x axis is τ'_e. The slope of the line fit to these points is the estimate for $2\gamma_3$. This approach of plotting many points together also provides a confidence check for the procedure itself: when a straight line closely fits the data points, the form of Eq. (6) is verified, indicating that the line shape of the transition is indeed Lorentzian.

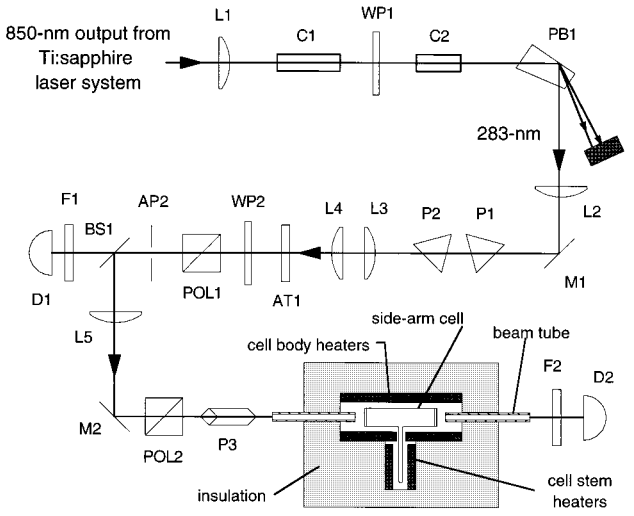

FIG. 2. Layout of the experimental apparatus for determining the linewidth of the one-photon $6s^26p^2\ {}^3P_0\rightarrow6s^26p7s\ {}^3P_1$ transition in ^{208}Pb.

In order to demonstrate this method, we constructed the apparatus shown in Fig. 2 to measure the linewidth of the $6s^26p^2\ {}^3P_0\rightarrow6s^26p7s\ {}^3P_1$ transition in atomic lead. The lead is contained in a commercially available [7] sealed fused-quartz sidearm cell. The body of the cell consists of a 4-in.-long, 1-in.-diam tube; optically flat windows are fused onto the ends of the tube and a 3-in.-long, $\frac{1}{4}$-in.-diam side arm is attached to the center of the tube. The cell is evacuated to approximately 1×10^{-5} Torr through the open end of the stem and baked for 24 h at 600 °C; after this bakeout, approximately 15 mg of metallic lead (isotopic purity 99.97% ^{208}Pb) is distilled through the stem and the stem is tipped off to seal the lead into the evacuated cell. Isotopically pure material is not required (see Sec. III); the cell was prepared for other experiments needing isotopically pure material and was reused for the present experiment.

The cell is heated in a furnace to approximately 800 °C. The furnace has two pairs of commercially available [8] split-tube-shaped heating elements that are used to keep the cell body approximately 30° warmer than the stem so that lead does not condense onto the windows. Ceramic, $\frac{1}{2}$-in.-diam beam tubes lead from the cell windows to past the furnace insulation in order to inhibit air currents transverse to the laser beam direction through the cell.

The lead vapor is probed by 283-nm laser pulses produced by frequency tripling the output of a pulsed, injection-seeded Ti:sapphire ring-laser system [9]. This system produces tunable, 14-ns-long laser pulses at 850 nm with a near Fourier-transform-limited linewidth. The laser pulses are focused by $L1$ to a spot near $C1$, a 1-cm-long lithium-borate (LBO) crystal cut for type-I phase matching to frequency double the 850-nm beam to 425 nm. The two beams emerge from this crystal and enter $C2$, a 7-mm-long β-barium-borate (BBO) crystal cut for type-I phase matching to produce a beam at 283 nm. The waveplate WP1, which

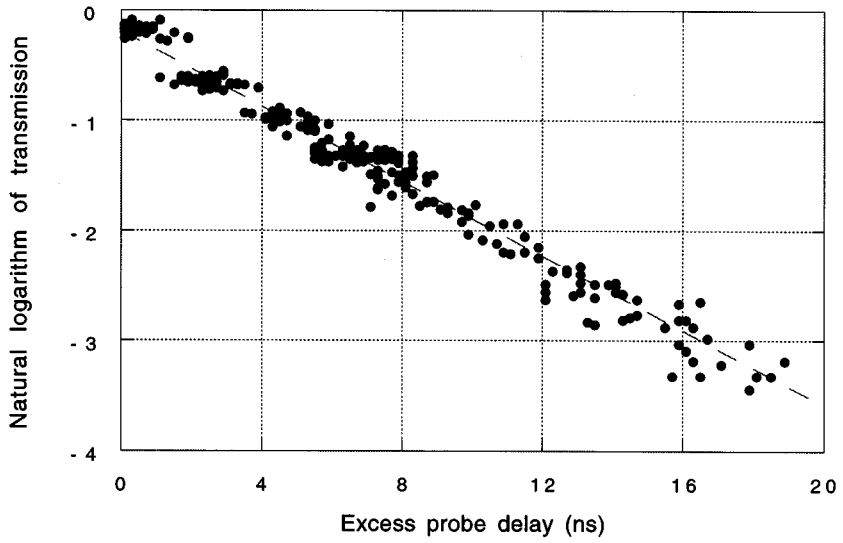

FIG. 3. Natural logarithm of the energy transmission of a series of pulses passed through the cell, plotted against their excess delay τ_e as the detuning of the pulses from line center of the transition is varied. The atom density is $N=1.5\times10^{14}$ atoms/cm^3. The slope of the dotted line fit by least squares to the data is 1.7×10^8 rad/s, which is the estimate for $2\gamma_3$.

produces a full-wave phase delay at 425 nm and a half-wave delay at 850 nm, is placed between the crystals in order to control the 283-nm intensity; by rotating the waveplate, the polarization of the 425-nm beam can be conveniently attenuated over several orders of magnitude.

The different wavelengths are separated by a Pellin-Broka prism PB1; the 425-nm and 850-nm beams are blocked and the 283-nm beam is collimated by $L2$ and given a circular profile by prisms $P1$ and $P2$. The beam is expanded by a telescope consisting of $L3$ and $L4$, passed through attenuator AT1, a half-wave plate WP2, through polarizer POL1, and through an aperture AP2. The waveplate is used with the polarizer as another stage of intensity control and the aperture, together with lens $L5$, sets the beam size in the cell to 0.2 mm (measured to the $1/e$ points). The attenuators are chosen so that the beam intensity in the cell is $\sim$100 mW/cm^2, which is well below the on-resonant saturation intensity ($\sim$500 mW/cm^2) of the lead resonance-line transition. By rotating the waveplates alone one can, without perturbing the beam alignment, reduce the beam intensity in the cell from a level that causes visible fluorescence on white paper down to the desired weak probing intensity; this feature is useful for aligning the beam. the polarizer POL2 fixes the beam polarization and the Fresnel rhomb $P3$ converts the polarization from linear to circular. Both the small beam size and the circular polarization are used in the latter portion of this work where the two-photon linewidth is measured; for consistency, they are used here as well, even though they are not required.

The beam is split at BS1 and passes through bandpass filter $F1$ to a 0.5-ns-rise-time photomultiplier detector $D1$ (Hamamatsu Model R5600U-03). The portion of the beam that emerges from the cell passes through bandpass filter $F2$ and onto a second fast photomultiplier $D2$. The signals from $D1$ and $D2$ are brought to a four-channel 5×10^9 sample/s Tektronix Model TDS 684A real-time digital oscilloscope, which simultaneously records the pulse wave forms. The wave forms are transferred to a computer that calculates the relative timing between the maxima of the two pulses in order to determine the propagation delay and calculates the ratio of the areas of the pulses in order to determine the energy transmission through the cell. The repetition rate of the pulses, 10 Hz, is determined by the laser that pumps the Ti:sapphire laser.

The results for ^{208}Pb are shown in Fig. 3. Each point in the plot represents the normalized attenuation and relative propagation delay of a single pulse at a particular detuning of the pulse center frequency ω_p from line center. The center frequency of the pulses is tuned over a range of approximately 1 cm^{-1} on one side of the line. As expected, the points fall near a straight line; the slope of this line is 1.7×10^8 rad/s, which is the estimate for $2\gamma_3$. From this value, the upper-state lifetime $\tau_3=1/2\gamma_3$ is estimated to be 5.9 ns, lying within the tolerances of other measured values [10]. We emphasize that it is not necessary to measure the optically frequency of the pulses; the only requirement is that the optical frequency be varied over a large enough range that there is a significant change in $\mathcal{E}_{\rm out}/\mathcal{E}_{\rm in}$ and τ_e.

The atom density N in the quartz cell can now be determined spectroscopically from the optical thickness of the $|1\rangle\rightarrow|3\rangle$ transition, which is found by measuring the transmission of probe laser pulses through the cell as a function of the laser frequency and by determining the frequency interval $\Delta\omega_{1/e}$, over which the transmission is less than $1/e$. This frequency range is typically very broad compared to the linewidth $2\gamma_3$ and is thus easy to measure with a standard commercial wavemeter. Assuming that the inhomogeneous linewidth is much less than $\Delta\omega_{1/e}$, Eq. (4) gives the relation between N and $\Delta\omega_{1/e}$:

$$N=\Delta\omega_{1/e}^2\frac{\epsilon_0\hbar c}{4|\mu_{13}|^2\gamma_3\omega_{31}L}. \tag{8}$$

A plot of the probe transmission as a function of its detuning from line center is shown in Fig. 4. From this plot, $\Delta\omega_{1/e}$ is 0.39 cm^{-1} and, using the $2\gamma_3$ determined above and the known matrix element ($\mu_{13}=-0.79$ a.u. for the circular polarization used), N is found to be 1.5×10^{14} atoms/cm^3.

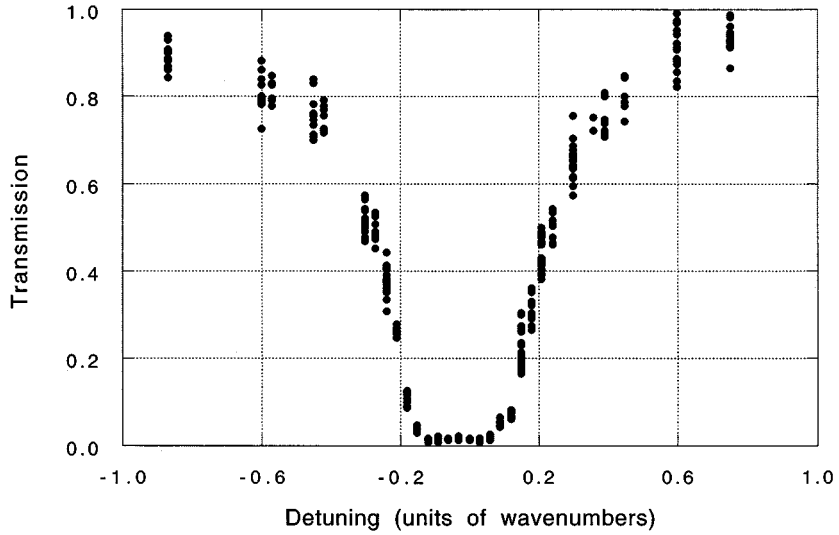

FIG. 4. Energy transmission of a series of pulses as a function of their detuning $\Delta\omega_p$. Using this figure and the linewidth determined in Fig. 3, the atom density is determined to be 1.5×10^{14} atoms/cm^3.

II. TWO-PHOTON METHOD

A schematic diagram of the system considered here is shown in Fig. 1(b). The system is based upon that of Fig. 1(a) with the addition of another state $|2\rangle$; our object is to determine the Lorentzian (FWHM) linewidth $2\gamma_2$ of the two-photon $|1\rangle\rightarrow|2\rangle$ transition. In addition to the probe field, we incorporate a second, ''coupling,'' monochromatic field $\mathcal{E}_c\exp(i\omega_c t)$ tuned near the center frequency ω_{32} of the $|2\rangle\rightarrow|3\rangle$ transition with detuning $\Delta\omega_c=\omega_{32}-\omega_c$. The Rabi frequencies of the probe and coupling fields on their respective transitions are given by $\Omega_p=|\mu_{13}\mathcal{E}_p|/\hbar$ and $\Omega_c=|\mu_{23}\mathcal{E}_c|/\hbar$, where μ_{23} is the matrix element of the $|2\rangle\rightarrow|3\rangle$ transition for the particular coupling field polarization used.

We assume that the coupling field intensity is much greater than the probe field intensity, so that $\Omega_c\gg\Omega_p$. The linear susceptibility of the medium as seen by the probe is then given by [11]

$$\chi(\omega_p)=\frac{|\mu_{13}|^2N}{\epsilon_0\hbar}\left[\frac{\Delta\tilde{\omega}_2}{\Delta\tilde{\omega}_2\Delta\tilde{\omega}_3-\dfrac{|\Omega_c|^2}{4}}\right], \tag{9}$$

where $\Delta\tilde{\omega}_2=(\Delta\omega_p-\Delta\omega_c)+j\gamma_2$ and $\Delta\tilde{\omega}_3=\Delta\omega_p+j\gamma_3$. We confine our attention to the case (discussed further in Sec. III) where Ω_c is sufficiently large that this equation can be simplified to

$$\chi(\omega_p)\simeq\frac{|\mu_{13}|^2N}{\epsilon_0\hbar}\left[\frac{-4(\Delta\omega_p-\Delta\omega_c)-4j\gamma_2}{|\Omega_c|^2}\right] \tag{10}$$

so that, using Eqs. (3) and (5), we obtain the absorption coefficient

$$\alpha=\frac{|\mu_{13}|^2N}{\epsilon_0\hbar}\frac{2\gamma_2\omega_{31}}{\Omega_c^2c} \tag{11}$$

and the excess group delay

$$\tau_e=\frac{|\mu_{13}|^2N}{\epsilon_0\hbar}\frac{2\omega_{31}L}{\Omega_c^2c}. \tag{12}$$

It immediately follows that

$$\ln(\mathcal{E}_{\rm out}/\mathcal{E}_{\rm in})=-2\gamma_2\tau_e. \tag{13}$$

This equation is analogous to Eq. (6) for one-photon transitions and can be interpreted in a similar way with the modification that the energy decay rate of the probe pulse is now $2\gamma_2$ instead of $2\gamma_3$. Physically, the energy of the pulse is (reversibly) contained in the coherent excitation of state $|2\rangle$ and in the coupling laser field [12]. State $|3\rangle$ is only infinitesimally excited (since the rate of change of the probe pulse is ''adiabatic'' [13]) and thus its decay rate is not important.

Since Eq. (13) does not contain Ω_c, the coupling field intensity does not, to a first approximation, need to be constant during the propagation of a probe pulse in order for the linewidth to be determined. This is of practical importance since, in order to achieve a sufficiently intense coupling field, the laser is often operated in a pulsed mode and thus, during the passage of the probe through the cell, the coupling laser intensity varies.

The experimental technique for determining $2\gamma_2$ is analogous to that for $2\gamma_3$, except that Ω_c is varied instead of $\Delta\omega_p$. By fitting $\ln(\mathcal{E}'_{\rm out}/\mathcal{E}'_{\rm in})$ vs τ'_e to a line and determining its slope, we determine $2\gamma_2$. To demonstrate this procedure, we determine the linewidth of the two-photon $6s^2 6p^2\ {}^3P_0\rightarrow 6s^2 6p^2\ {}^3P_2$ transition in atomic lead, using as an intermediate state the upper state of the one-photon transition discussed above. The experimental apparatus is shown in Fig. 5; the portion that produces the 283-nm beam is omitted since it is unchanged from the one-photon experiment; the cell and furnace are also unchanged.

A second seeded Ti:sapphire laser system produces 812-nm pulses that are focused by $L6$ to a spot near a 7-mm-long BBO crystal ($C3$) cut for type-I phase matching in order to produce a 406-nm beam. The 406-nm beam is given a circular profile by cylindrical lens $L7$ and is then collimated by $L8$ so that the beam size in the cell is 1 mm. The waveplate WP3 rotates the linear 812-nm beam polarization

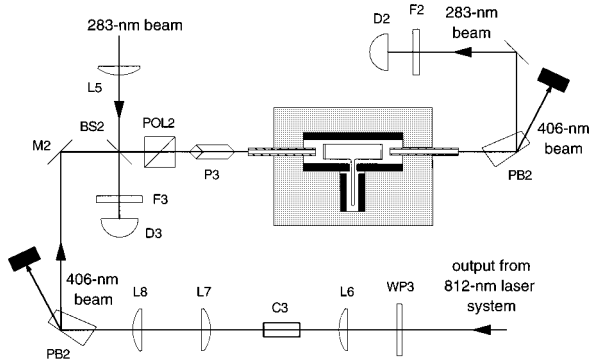

FIG. 5. Layout of the apparatus for determining the linewidth of the two-photon $6s^2 6p^2\ ^3P_0 \rightarrow 6s^2 6p^2\ ^3P_2$ transition in ^{208}Pb. The 283-nm beam is produced by part of the appartus shown in Fig. 2.

out of the c axis of $C3$, thus controlling the intensity of the 406-nm radiation in the same manner that WP1 controls the intensity of the 283-nm radiation. A Pellin-Broka prism PB2 separates the 406-nm from the 812-nm beam, which is blocked. The 406-nm beam is reflected by $M2$ into BS2 (at the position occupied by $M2$ in the one-photon-experiment apparatus), which combines the 283-nm and 406-nm beams. The portion of the 406-nm beam that reflects from BS2 passes through bandpass filter $F3$ and enters a third fast photodetector whose signal goes to the same oscilloscope monitoring the signals from $D1$ and $D2$. POL2 and $P3$ ensure that the beams have opposite circular polarization before entering the cell. A Pellin-Broka prism placed after the cell separates the 406-nm and 283-nm beams; the 283-nm beam travels through a bandpass filter to the photomultiplier $D2$ and the 406-nm beam is blocked.

The coupling and probe laser pulses must overlap in both space and time. In order to ensure good temporal overlap, the coupling pulse is timed to enter the cell before the probe pulse and it is of sufficient duration that it remains present until after the probe pulse has left the cell. The coupling laser pulse duration (100 ns) is thus intentionally made significantly longer than the probe laser pulse; to accomplish this, the 812-nm laser cavity round-trip distance is made very long (2 m) compared to the 40-cm round-trip distance of the 850-nm laser cavity.

In order to ensure that the transverse portions of the probe beam travel together with the same group velocity, the coupling laser intensity must be uniform across the probe beam. The probe beam, focused to a 0.2-mm-diam spot (measured to the $1/e$ intensity points) in the cell, is thus centered on the 0.9-mm-diam coupling laser beam so that the coupling laser intensity varies by only a few percent across the probe beam.

The data collection in this experiment is similar to the setup for the one-photon experiment with the addition of a fast photodiode (PD3) to monitor the coupling laser intensity. As before, the wave forms are transferred to a computer that calculates, on a shot-to-shot basis, $\ln(\mathcal{E}'_{\rm out}/\mathcal{E}'_{\rm in})$ and τ'_e. In order to reduce the effect of fluctuation in the relative arrival times of the probe and coupling lasers, the computer retains only wave forms where the probe pulse peak arrives at the cell within 16–30 ns before the coupling pulse peak. The coupling laser amplitude is calibrated in $\rm cm^{-1}$ by using the method described in Ref. [1].

The results for ^{208}Pb are shown in Fig. 6. These data are the same as those used in Ref. [1]. The plot is analogous to Fig. 3, where each point in the plot represents the normalized attenuation and relative propagation delay of a single probe pulse overlapped by a particular coupling laser pulse. The peak coupling laser intensity is varied from pulse to pulse by turning the intensity-control waveplate as the pulses are recorded. In this plot, the peak coupling laser Rabi frequency varies from 0.5 $\rm cm^{-1}$ on the left to 0.15 $\rm cm^{-1}$ on the right. As expected, the points fall around a straight line; the slope of this line is 1.0×10^7 rad/s, which is the first-order estimate for $2\gamma_2$. In Sec. III, this estimate is refined to 8.3×10^6 rad/s by compensating for the Doppler effect.

In this experiment, the atom density (determined using the method of Sec. I) is 2×10^{14} atoms/$\rm cm^3$ and the $|1\rangle\rightarrow|3\rangle$ transition linewidth is $2\gamma_3 = 1.9\times10^8$ rad/s, which is broader by 2×10^7 rad/s than the value determined in Sec. I. We believe that collisional broadening from a small amount of ''foreign'' gas, either outgassed from the cell walls or liberated from impurities inadvertently distilled into the cell, is responsible for this increase in linewidth. The cell had been at 800 °C for only a few hours when the data of Sec. I were acquired, but had been hot for 20–30 h when the data in the present section were taken.

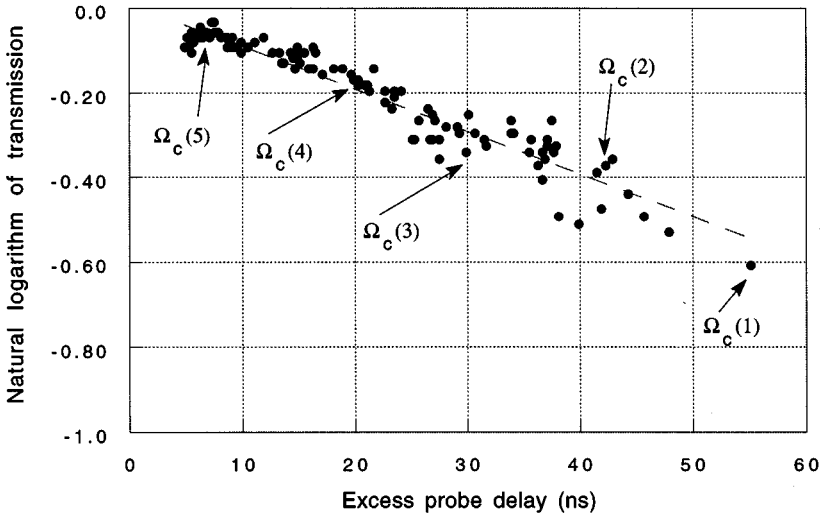

FIG. 6. Natural logarithm of the energy transmission of a series of pulses plotted against their excess delay τ_e as the coupling Rabi frequency Ω_c is varied. The atom density is $N=2\times10^{14}$ atoms/$\rm cm^3$, as determined by the method described in Sec. I. The slope of the line fit to this data is 1.0×10^7 rad/s and is the first-order experimental estimate of the Lorentzian FWHM linewidth $2\gamma_2$ of the $6s^2 6p^2\ ^3P_0 \rightarrow 6s^2 6p^2\ ^3P_2$ transition in our 10-cm-long ^{208}Pb cell at 800 °C. For reference, various data points are labeled with the peak Rabi frequency experienced by the pulse: $\Omega_c(1)=0.15\ \rm cm^{-1}$, $\Omega_c(2)=0.17\ \rm cm^{-1}$, $\Omega_c(3)=0.19\ \rm cm^{-1}$, $\Omega_c(4)=0.25\ \rm cm^{-1}$, and $\Omega_c(5)=0.5\ \rm cm^{-1}$.

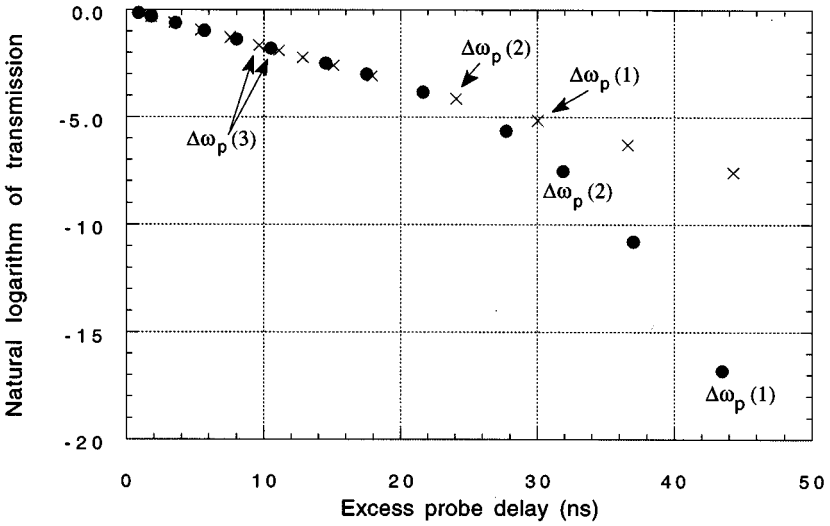

FIG. 7. Numerical simulation of the experiment to determine the Lorentzian linewidth of the $6s^2 6p^2\ ^3P_0 \rightarrow 6s^2 6p 7s^3 P_1$ transition in atomic lead. Here $2\gamma_3 = 1.7\times 10^8$ rad/s, $N = 1.5\times 10^{14}$ atoms/cm^3, and (for circular polarization) the transition matrix element is $\mu_{13} = -0.79$ a.u. The crosses represent the natural logarithm of the energy transmission plotted vs the excess delay of pulses traveling through the medium with no inhomogeneous linewidth included in the simulation. The solid dots are as above, except that they allow for the inclusion of the inhomogeneous linewidth from the Doppler effect at $T = 800$ °C. Various points are labeled with their respective detunings: $\Delta\omega_p(1) = 0.085$ cm^{-1}, $\Delta\omega_p(2) = 0.095$ cm^{-1}, and $\Delta\omega_p(3) = 0.15$ cm^{-1}. Data points for which $\tau_e > 30$ ns do not fit the line determining $2\gamma_3$.

The foreign gas is also probably responsible for the value of $2\gamma_2$ we measured, as the natural lifetime of this metastable transition is very much larger than the 100-ns coherence time implied by our measurement of $2\gamma_2$. Further evidence for the presence of foreign gas broadening of both transitions is provided by noting that the 2×10^7 rad/s excess linewidth of the $|1\rangle \rightarrow |3\rangle$ transition is close to the 8.3×10^6 rad/s linewidth of the $|1\rangle \rightarrow |2\rangle$ transition, which is typical behavior of nonresonant collisional broadening [15]. Moreover, after the cell is maintained for many days at 800 °C, both transitions continue to broaden, but the ratio of these linewidths remains nearly the same.

III. DISCUSSION: CONDITIONS AND LIMITATIONS ON THE GROUP-VELOCITY METHOD

We now discuss the limitations for determining the linewidth of one-photon transitions and then present the limitations for two-photon transitions.

A. One-photon transitions

The central assumption made in the analysis leading to Eq. (6) is that the homogeneous transition line shape is Lorentzian. In systems where the transition is broadened only by the natural lifetime of the states, this assumption is valid; however, when the transition is collisionally broadened, the assumption of a Lorentzian linewidth is not necessarily valid. In general, for systems with gas pressures less than 100 Torr, a Lorentzian linewidth can be assumed since, in this regime, it is valid to make the impact approximation for the collision dynamics [4].

In dilute media, it is tempting to tune the laser pulses very close to line center since, according to Eqs. (4) and (5), α and $1/v_g$ increase rapidly as $\Delta\omega_p$ becomes small and it is easier to accurately fit the line determining $2\gamma_3$ to wide-ranging data. There is, however, a lower bound to $\Delta\omega_p$ below which Eq. (1) becomes inaccurate; this bound is determined by the inhomogeneous linewidth of the transition. In the case of a gaseous medium, the inhomogeneous linewidth is due to the Doppler effect: the atoms are not stationary in the direction of the probe laser and have randomly distributed velocities so that ω_3 is different for each atom. In order to calculate the correct χ it is necessary to replace ω_3 by $\omega_3(1+v_x/c)$ in Eq. (1) (where v_x is the atom velocity in the direction of the probe laser) and to integrate over the Maxwell-Boltzmann distribution of v_x. In order to calculate the conditions under which Eq. (4) is accurate, we separate $\Delta\omega_p$ into $\Delta\omega_p = \Delta\omega_{p,0} + \Delta\omega_{p,v_x}$, where $\Delta\omega_{p,0}$ is the detuning from the $v_x = 0$ velocity class and $\Delta\omega_{p,v_x}$ is the additional detuning from the class with velocity v_x, and expand Eq. (1) in a power series $\Delta\omega_{p,v_x}/\Delta\omega_{p,0}$. The first term of this expansion gives Eq. (4). Analytically integrating the second term over the Doppler distribution, we find it negligible in comparison with the first term when

$$\Delta\omega_{p,0} \gg \gamma_3, \Delta\omega_{D3}, \tag{14}$$

where $\Delta\omega_{D3}$ is the FWHM Doppler width of the $|1\rangle \rightarrow |3\rangle$ transition.

In order to study the effect of finite $\Delta\omega_p$, we have numerically integrated Eq. (1) over the Doppler distribution for the parameters of this experiment. Figure 7 shows $\ln(\mathcal{E}_{\text{out}}/\mathcal{E}_{\text{in}})$ plotted vs τ_e as $\Delta\omega_p$ is varied, both with and without taking into account the inhomogeneous linewidth. This and the simulations shown in Sec. III B, are performed using an adaptive step-size Runge-Kutta algorithm [14]. For $\Delta\omega_p > 0.1$ cm^{-1} (1.8 times the FWHM Doppler linewidth), the points for the system with inhomogeneous broadening

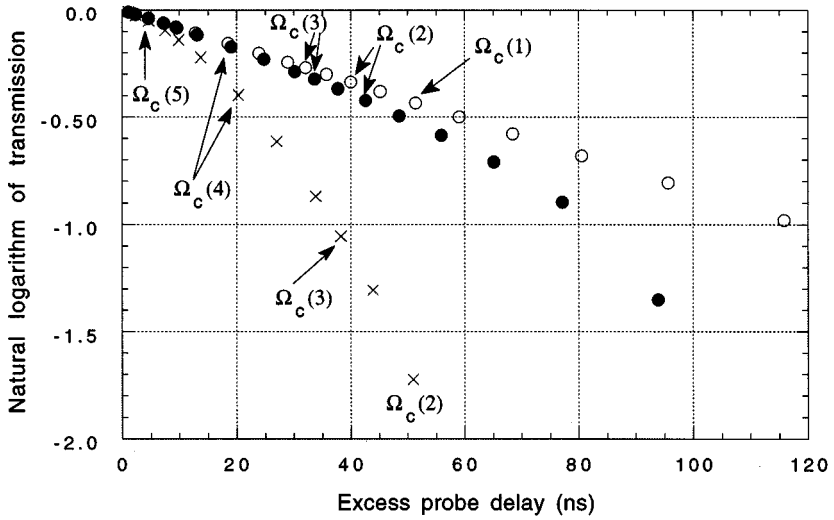

FIG. 8. Numerical simulation of the experiment to determine the Lorentzian linewidth of the two-photon $6s^2 6p^2\ ^3P_0 \rightarrow 6s^2 6p^2\ ^3P_2$ transition in atomic lead using the parameters $N=2\times10^{14}$ atoms/cm^3, $2\gamma_3=1.9\times10^8$ rad/s, and $2\gamma_2=8.3\times10^6$ rad/s. The data points represent the natural logarithm of the energy transmission and the excess delay plotted together for a series of pulses as the coupling Rabi frequency Ω_c is varied. The clear dots are calculated for a system free from inhomogeneous linewidth and the solid dots are calculated for the inhomogeneous linewidth produced by the Doppler effect at $T=800\,^\circ$C. The points marked by crosses result when the two-photon detuning is $\Delta\omega_p-\Delta\omega_c=0.03$ cm^{-1}. For excess delay under 50 ns, both the solid and the clear dots lie near the same line, but for longer delays the points with inhomogeneous broadening taken into account fall away. The results for nonzero detuning do not lie close to a straight line until $\Omega_c>0.5$ cm^{-1}. For reference and for comparison with the experimental data of Fig. 6, various points are labeled with their Rabi frequencies: $\Omega_c(1)=0.15$ cm^{-1}, $\Omega_c(2)=0.17$ cm^{-1}, $\Omega_c(3)=0.19$ cm^{-1}, $\Omega_c(4)=0.25$ cm^{-1}, and $\Omega_c(5)=0.5$ cm^{-1}.

included in the calculation lie near the line determining $2\gamma_3$, which indicates a practical lower bound for $\Delta\omega_p$.

Although the analysis and experiments presented in this paper have focused on a single-isotope atomic medium (with no hyperfine structure), this is not a necessary restriction. In media made up of a variety of constituents (possibly exhibiting hyperfine structure), the $|1\rangle\rightarrow|3\rangle$ transition seen by the probe becomes a family of nearby transitions. Insofar as each of these transitions has equal linewidth, the method works as long as the laser detuning satisfies Eq. (14) for each transition.

In order for a probe pulse to travel through the medium without distortion, its frequency components must all travel through the medium with nearly the same group velocity and energy transmission. Since distortion is not readily quantified and depends upon the details of the input pulse shape, we can only approximate its lower bound. For a pulse of detuning $\Delta\omega_p$ and equivalent duration [16] Δt satisfying

$$\Delta t > \frac{10}{\Delta\omega_p}, \tag{15}$$

v_g, for the frequency components within its equivalent bandwidth, varies by no more than 10%. In the present experiment, we are thus constrained to $\Delta t>0.6$ ns. In practice, for probe pulse lengths near this bound, one should repeat the measurement of $2\gamma_3$ for different pulse lengths and verify that they yield the same estimate for $2\gamma_3$. A more detailed analysis of this effect is given in Ref. [5].

It is important to note that this technique may be used to measure the linewidth of transiently populated, excited-state transitions. The reason for this is that the population N is absent from Eq. (6), which means that N may vary from pulse to pulse or even vary as the pulse traverses the medium. In any case, as noted above, N need not be measured.

B. Two-photon transitions

In order to accurately determine $2\gamma_2$, it is necessary for the experiment to satisfy all of the conditions implicit in the derivation of Eq. (13). In particular, ω_2 and ω_3 are assumed to be fixed and resonant with all of the atoms in the medium, Ω_c is assumed to be constant while the pulse travels through the medium, and both lasers are assumed to be monochromatic.

If the atomic transitions are inhomogeneously broadened, ω_2 and ω_3 are no longer fixed for all the atoms in the medium; this effect must be considered when we determine the conditions under which Eq. (9) can be accurately approximated with Eq. (10). Making the approximation $|\Omega_c|^2 \gg 4|\Delta\tilde{\omega}_2\Delta\tilde{\omega}_3|$ and expanding Eq. (9) in a power series, we obtain

$$\chi(\omega_p)=\frac{|\mu_{13}|^2 N}{\epsilon_0\hbar}\left[\frac{-4\Delta\tilde{\omega}_2}{|\Omega_c|^2}-\frac{16\Delta\tilde{\omega}_2^2\Delta\tilde{\omega}_3}{|\Omega_c|^4}+\cdots\right]. \tag{16}$$

We now determine the conditions under which we may drop all terms in this series beyond the first, yielding Eq. (10). Defining $\Delta\omega_{D2}$ as the Doppler linewidth of the $|1\rangle\rightarrow|2\rangle$ transition and integrating the first two terms of Eq. (16) over the Doppler distribution, we find that the contribution of the first term to the susceptibility is dominant when

$$|\Omega_c|^2 \gg \max[4\gamma_2\gamma_3, \Delta\omega_{D2}\Delta\omega_{D3}, (\gamma_3/\gamma_2)\Delta\omega_{D2}^2]. \tag{17}$$

In the case of our experiment, $(\gamma_3/\gamma_2)\Delta\omega_{D2}^2$ is largest and equals $(0.08\ \mathrm{cm}^{-1})^2$.

Due to pulse-to-pulse fluctuations, it is desirable to acquire data with a large spread in $\ln(\mathcal{E}'_{\mathrm{out}}/\mathcal{E}'_{\mathrm{in}})$ and τ'_e. This is accomplished by varying Ω_c over a wide range, but practical limitations (beam uniformity and laser power) set an upper limit on Ω_c so that, in practice, one may approach the bound of Eq. (17), as is the case with the present experiment. In order to refine our estimate for $2\gamma_2$, we numerically simulate the experiment by integrating Eq. (9) over the Doppler-induced distribution of ω_2 and ω_3, using the parameters of our experiment and various trial values for $2\gamma_2$, until the slope of the line fit to the results matches that found in the experiment. In this way, we refine the estimate for $2\gamma_2$ to 8.3×10^6 rad/s (a 20% correction).

Another important limitation on the accuracy of this method for determining two-photon linewidths is the detuning of the lasers from resonance. Estimating the detuning for which the imaginary term of Eq. (9) doubles, we get

$$\Delta\omega_p - \Delta\omega_c \ll \frac{\Omega_c}{2}\left(\frac{\gamma_2}{\gamma_3}\right)^{1/2}. \tag{18}$$

In order to illustrate the effect of detuning, we numerically simulate the experiment using the measured values for $2\gamma_3$, $2\gamma_2$, N, and T. The results are shown in Fig. 8, where three sets of data are plotted: (1) circles correspond to the case where no inhomogeneous broadening is present ($T=0$ K) and both lasers are resonant (for the other data sets, inhomogeneous broadening corresponding to $T=800$ °C is present), (2) dots correspond to the case where both lasers are resonant, and (3) crosses correspond to the case where $\Delta\omega_p - \Delta\omega_c = 0.03\ \mathrm{cm}^{-1}$ and $\Delta\omega_p = 0$. From Eq. (18), the Rabi frequency must exceed $0.3\ \mathrm{cm}^{-1}$ in order to use the two-photon method with 0.03-cm^{-1} wave numbers of detuning; we see, in Fig. 8, the result when this condition is not met: a much larger apparent linewidth is measured. We have observed this result experimentally: when our lasers are detuned, the measured value of $2\gamma_2$ always exceeds the correct value.

In media made up of a variety of isotopes, the method can still be applied, provided that Eq. (18) is satisfied for each of the isotopes. In the case of isotopes with hyperfine structure, $\Delta\omega_p$ and $\Delta\omega_c$ in Eq. (18) are replaced by the hyperfine splittings of states $|3\rangle$ and $|2\rangle$, respectively. Situations where Eq. (18) is not satisfied are discussed in [17].

The expression given by χ in Eq. (9) assumes, in addition to the absence of an inhomogeneous linewidth, that the lasers used are monochromatic. As in the case of the one-photon method, the probe pulse can be represented as a superposition of monochromatic radiation with most of the energy distributed in a frequency band of width $\delta\omega_p$ about the center frequency ω_3. As long as the values calculated for α and v_g do not vary significantly for frequencies within this band, we can neglect the effect of finite pulsewidth. From inequality (18) above, the absorption coefficient approximately doubles when $\Delta\omega_p$ increases from 0 to $(\Omega_c/2)\sqrt{\gamma_2/\gamma_3}$; τ_e is relatively unchanged. The bandwidth of the probe pulses must therefore satisfy $\delta\omega_p \ll \Omega_c\sqrt{\gamma_2/\gamma_3}$. In the case of the 14-ns-long pulses used in our experiment, $\delta\omega_p \approx \frac{1}{50}\Omega_c\sqrt{\gamma_2/\gamma_3}$.

The effect of a nonmonochromatic Ω_c is more subtle than for a nonmonochromatic probe pulse. Numerical simulations indicate that probe pulses travel free from distortion when the coupling laser pulse width (FWHM) exceeds the transit time of the probe pulse in the cell and the probe ''sees'' the rising and falling edges of the coupling laser for equal times. If, however, the probe pulse sees only a rising (falling) coupling laser intensity, the front edge of the pulse experiences a longer (shorter) excess delay than the back edge since, according to Eq. (12), τ_e varies as the inverse square of Ω_c. As a consequence, the probe pulse shape changes. This effect is especially pronounced when the total propagation delay of the probe pulse through the medium is on the same scale as the coupling laser pulse width. Due to unavoidable jitter in the timing of pulsed lasers, the result is that data become noisy for longer propagation delays, an effect that is discernible in Fig. 6 and discussed in more detail in Ref. [1].

CONCLUSION

In summary, we have presented two methods for determining one- and two-photon Lorentzian linewidths and applied these methods to a ^{208}Pb atomic medium. The techniques do not require precise knowledge of the atom density, laser frequency, or matrix elements and are reasonably simple to use. As an additional benefit, with the Lorentzian linewidth of a one-photon transition determined, the number density of a medium can be robustly determined as well.

ACKNOWLEDGMENTS

The authors gratefully acknowledge contributions by A. Merriam and H. Xia. This work was supported by the U.S. Office of Naval Research, the U.S. Army Research Office, and the U.S. Air Force Office of Scientific Research.

[1] A Kasapi, M. Jain, G. Y. Yin, and S. E. Harris, Phys. Rev. Lett. **74**, 2447 (1995).

[2] A. E. Siegman, *Lasers* (University Science Books, Mill Valley, CA, 1986).

[3] M. Sargent III, M. O. Scully, and W. E. Lamb, Jr., *Laser Physics* (Addison-Wesley, Reading, MA, 1974).

[4] A. Corney, *Atomic and Laser Spectroscopy* (Clarendon, Oxford, 1977).

[5] S. E. Harris, J. E. Field, and A. Kasapi, Phys. Rev. A **46**, R29 (1992).

[6] D. Grischkowski, Phys. Rev. A **7**, 2096 (1973).

[7] Opthos Instruments, Inc. Rockville, MD.

[8] Thermocraft Inc, Winston-Salem, NC.
[9] A. Kasapi, G. Y. Yin, and M. Jain, Appl. Opt. **35**, 1999 (1996).
[10] D. H. Griers, J. B. Atkinson, and L. Krause, Can. J. Phys. **62**, 1616 (1984).
[11] S. E. Harris, J. E. Field, and A. Imamoglu, Phys. Rev. Lett. **64**, 1107 (1990).
[12] H. R. Gray, R. M. Whitley, and C. R. Stroud, Jr., Opt. Lett. **3**, 218 (1978); E. Arimondo and G. Orriols, Nuovo Cimento Lett. **17**, 333 (1976); G. Orriols, Nuovo Cimento B **53**, 1 (1979).
[13] J. R. Kuklinski, U. Gaubatz, F. T. Hioe, and K. Bergmann, Phys. Rev. A **40**, 6741 (1989).
[14] W. H. Press, B. P. Flannery, S. A. Teukolski, and W. T. Vetterling, *Numerical Recipes in C* (Cambridge University Press, New York, 1988).
[15] W. R. Hindmarch and J. M. Farr, *Collisional Broadening of Spectral Lines by Neutral Atoms* (Pergamon, New York, 1972).
[16] R. N. Bracewell, *The Fourier Transform and Its Applications* (McGraw-Hill, New York, 1986).
[17] A. Kasapi (unpublished).